ACS APPLIED MATERIALS & INTERFACES

Research Article

www.acsami.org

Nitrogen-Doped Graphene Nanoribbons as Efficient Metal-Free Electrocatalysts for Oxygen Reduction

Mingkai Liu,[†] Yanfang Song,[‡] Sixin He,[†] Weng Weei Tjiu,[§] Jisheng Pan,[§] Yong-Yao Xia,[‡] and Tianxi Liu*,[†]

[†]State Key Laboratory of Molecular Engineering of Polymers, Department of Macromolecular Science, Fudan University, Shanghai 200433, China

[‡]Department of Chemistry and Shanghai Key Laboratory of Molecular Catalysis and Innovative Materials, Institute of New Energy, Fudan University, Shanghai 200433, P. R. China

[§]Institute of Materials Research and Engineering, A*STAR (Agency for Science, Technology and Research), 3 Research Link, Singapore 117602, Singapore

Supporting Information

ABSTRACT: Nitrogen-doped graphene nanoribbon (N-GNR) nanomaterials with different nitrogen contents have been facilely prepared via high temperature pyrolysis of graphene nanoribbons (GNR)/polyaniline (PANI) composites. Here, the GNRs with excellent surface integration were prepared by longitudinally unzipping the multiwalled carbon nanotubes. With a high length-to-width ratio, the GNR sheets are prone to form a conductive network by connecting end-to-end to facilitate the transfer of electrons. Different amounts of PANI acting as a N source were deposited on the surface of GNRs via a layer-by-layer approach, resulting in the formation of N-GNR nanomaterials with different N contents after being pyrolyzed. Electrochemical characterizations reveal that the obtained $N_{8.3}$-GNR nanomaterial has excellent catalytic activity toward an oxygen reduction reaction (ORR) in an alkaline electrolyte, including large kinetic-limiting current density and long-term stability as well as a desirable four-electron pathway for the formation of water. These superior properties make the N-GNR nanomaterials a promising kind of cathode catalyst for alkaline fuel cell applications.

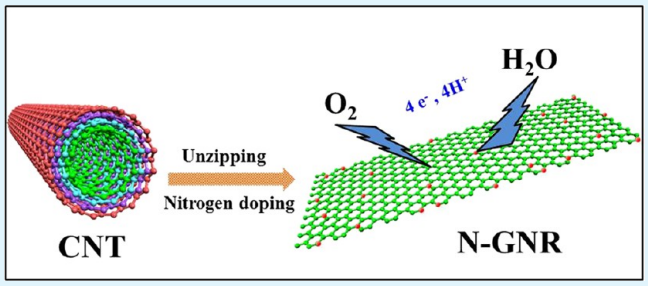

KEYWORDS: *graphene nanoribbon, nitrogen-doped, electrocatalysts, oxygen reduction reaction*

1. INTRODUCTION

Graphene nanoribbons (GNRs), as a novel carbonic material, have attracted intensive attention due to their superior physical and chemical properties. Generally, GNRs can be organically fabricated by a bottom-up approach or longitudinally unzipping single- or multiwalled carbon nanotubes (CNTs).[1,2] Although other methods, such as lithographic,[3] chemical,[4] and chemical vapor deposition (CVD),[5] can produce a microscopic specimen of GNRs, they cannot be utilized to prepare GNRs with smooth edges and controlled width at high yield. The obtained GNRs produced by longitudinally unzipping from the carbon nanotubes not only have the unique characteristic of graphene such as lightweight, high thermal conductivity, superior mechanical properties, and electronic transport properties but also possess particular features such as high length-to-width ratio, straight edges, and excellent surface integration with less defects and/or holes on the basal plane.[6,7] These unique characteristics make GNRs promising candidates in various practical applications such as field-effect transistors, transparent electrodes, hydrogen storage, and polymer composites.[6,8−11]

Although the surface integration endows graphene or GNRs with excellent physical properties such as electrical conductivity and thermal transmission, the chemically stable sp^2 hybridized carbon atoms in graphene and the GNR framework hinder their further applications in chemistry, particularly in catalysis. Up to now, many strategies have been employed to tailor or modify the electronic properties of graphene via chemical or physical methods.[12−16] Both theoretical calculations and experiments have proved that chemical doping with heteroatoms like N and B can intrinsically modify the properties of carbon materials.[14] Especially, the N atom is considered as the best candidate for carbon substitution because it has five valence electrons which are prone to form strong valence bonds with carbon atoms. In addition, the lone electron pairs of N atom can provide "electrocatalytically active sites" in graphene framework after being hybridized with sp^2 carbon atoms, which will considerably enhance the reactivity and electrocatalytic

Received: December 20, 2013
Accepted: February 24, 2014
Published: February 24, 2014

   dx.doi.org/10.1021/am405900r | ACS Appl. Mater. Interfaces 2014, 6, 4214−4222

performance of graphene.[17,18] Dai and co-workers prepared a kind of N-doped carbon nanotube arrays which were produced by pyrolysis of iron phthalocyanine (a metal heterocyclic molecule containing nitrogen) and subsequent removal of the residual Fe catalyst by electrochemical purification. This catalyst exhibits a much better electrocatalytic activity, long-term operation stability, and tolerance to crossover effect than platinum of oxygen reduction reaction (ORR) in alkaline fuel cells.[19] Also, Wong and co-workers prepared a nanoporous few-layer nitrogen-doped graphene by high-temperature pyrolysis of the composite of graphene oxide and polyaniline.[20] The resulting catalyst contains 2.4 wt % nitrogen element and exhibits large kinetic-limiting current density, long-term stability, and a desirable four-electron pathway for the formation of water. Furthermore, Dai and co-workers developed an oxygen reduction electrocatalyst based on carbon nanotube-graphene complexes. After being annealed in ammonia atmosphere at high temperature, the prepared catalysts exhibit high activity, excellent tolerance to methanol, and superior stability in comparison to other nonprecious metal catalysts in both acidic and alkaline solutions.[21] In this work, GNRs were prepared by longitudinally unzipping of multiwalled CNTs, and nitrogen-doped GNR (N-GNR) nanomaterials have been successfully prepared by high-temperature pyrolysis of GNR/polyaniline (GNR/PNAI) composites, where PANI was controllably deposited on the surface of GNR sheets as a nitrogen source. In this way, N-GNR nanomaterials with nitrogen contents from 4.1 wt % to 8.3 wt % have been obtained by adjusting the weight percentage of PANI in the GNR/PANI composites. Being used as metal-free ORR electrocatalysts, the N-GNR materials exhibit excellent activity with an electron transfer number of 3.91 and superior stability compared to the commercial Pt/C electrocatalyst in alkaline medium, which makes them promising catalysts in electrochemical applications.

2. EXPERIMENTAL SECTION

Materials. Multiwalled CNTs used in this work are commercially obtained from Chengdu Organic Chemicals Co. Ltd., which are produced by the CVD method with a diameter of 30−50 nm and a length of about 30 μm. Aniline monomer and ammonium persulfate (APS) were purchased from Sinopharm Chemical Reagent Co. Ltd., and Milli-Q ultraclean water was used throughout the experiments. The commercial Pt/C catalyst (20 wt %) was purchased from Sigma-Aldrich. All other reactants were directly used without any further purification.

Preparation of GNR Sheets and N-GNR Nanomaterials. Graphene nanoribbons were prepared by longitudinally unzipping the multiwalled CNTs. Typically, 200 mg of pristine CNTs was suspended in 45 mL of concentrated sulfuric acid (H_2SO_4) in a flask and stirred for 1 h to form a uniformly dispersed solution. Then, 6 mL of phosphoric acid (H_3PO_4) was added dropwise, and the mixture was allowed to stir for another 30 min at room temperature. After that, the reaction temperature was increased to 70 °C, and 1 g of potassium permanganate ($KMnO_4$) was gradually added into the reaction mixture, in which $KMnO_4$ was added by 200 mg per hour until it was used out. After being cooled to room temperature naturally, the mixture was poured into 250 mL of ice−water containing 10 mL of hydrogen peroxide (H_2O_2) (30 wt %) and allowed to coagulate for 24 h. Then the obtained precipitate was sonicated for 30 min at 250 W and dialyzed against ultraclean water for 1 week to get a solution with good dispersion of the oxided GNR sheets, which was further reduced by hydrazine hydrate at 98 °C with stirring for 3 h, resulting in the formation of pure GNR sheets. A certain amount of aniline monomer (from 20, 50, 100 to 200 mg) was codispersed with GNRs (100 mg) in 50 mL of 1 M HCl solution in a flask, and 40 mL of 1 M HCl solution containing 2 times the amount of APS was slowly added into the flask dropwise to get the composites of GNRs and polyaniline (PANI), denoted as GNR-$PANI_{20}$, GNR-$PANI_{50}$, GNR-$PANI_{100}$, and GNR-$PANI_{200}$, respectively. N-GNR nanomaterials with different N contents were prepared by pyrolyzing GNR/PANI composites at 900 °C for 1 h in an argon atmosphere. For comparison, pure GNR sheets without PANI were also treated with the same pyrolysis process and used as a reference sample.

Characterization. Transmission electron microscopy (TEM) images were obtained on a Philips CM300 FEG TEM instrument operated under an acceleration voltage of 200 kV. X-ray diffraction (XRD) measurements were carried out using a PANalytical X'Pert PRO XRD with Cu Kα radiation (λ = 0.1542 nm; operating voltage, 40 keV; cathode current, 40 mA; scan rate, 2° min^{-1}). Scanning electron microscopy (SEM) images were observed by a field emission scanning electron microscope (FESEM, JEOL JSM-6700 F). Raman spectra were collected using an Avalon Instruments Raman Station with a 632.8 nm He−Ne laser. X-ray photoelectron spectroscopy (XPS) spectra were collected by a Perkin-Elmer PHI 5000 CESCA spectrometer equipped with a hemispherical electron energy analyzer at a pressure lower than 1029 Torr. Fourier transform infrared (FTIR) spectra were obtained from a Nicolet Nexus 470 infrared spectrophotometer with a scan range of 400−4000 cm^{-1} and signal-averaging 64 scans at a resolution of 4 cm^{-1}.

Electrochemical Characterizations. The electrochemical properties of N-GNR nanomaterials were tested in a three-electrode system, in which a Pt wire and an Ag/AgCl electrode filled with a saturated KCl aqueous solution were used as the counter electrode and reference electrode, respectively. A glass carbon electrode with a diameter of 3 mm was used as a working electrode which was mechanically polished with 1.0, 0.3, and 0.05 μm alumina slurry and washed with ultraclean water and ethanol to get a mirrorlike surface. Twenty mg of the N-GNR sample was dispersed in a 10 mL solvent mixture of Nafion (5%) and water (v/v ratio = 1:9) using sonication. Five μL of the prepared suspension was dropped onto the glass carbon electrode (3 mm diameter, 0.07065 cm^2 geometric area). Nitrogen (N_2) or oxygen (O_2) was used to purge the solution to achieve the N_2 or the O_2-saturated electrolyte. The Pt/C catalyst (20 wt %) was used for comparison. All the samples were tested for 5 times at least. CV and RDE experiments were carried out at a scan rate of 10 mV/s during the potential of +0.2 to −0.8 V in 0.1 M KOH solution.

The RDE measurements were carried out at different rotating speeds between 400 and 2400 rpm in the O_2-saturated 0.1 M KOH aqueous solution. The Koutecky−Levich plots (J^{-1} vs $\omega^{-1/2}$) were analyzed at various electrode potentials. The slopes of their linear fit lines are used to calculate the electron transfer number (n) on the basis of the Koutecky−Levich equation

$$\frac{1}{J} = \frac{1}{J_K} + \frac{1}{J_L} = \frac{1}{J_K} + \frac{1}{B\omega^{1/2}}$$

where J is the measured current density, J_K is the kinetic current density of the ORR, and ω is the angular velocity of rotation. Here, B is related to the diffusion-limited current density through the expression $J_L = B\omega^{1/2}$, which can be defined as

$$B = 0.62nFv^{-1/6}D_{O_2}{}^{2/3}C_{O_2}$$

where n is the overall number of electrons transferred during the oxygen reduction, F is the Faraday constant (96485 C mol^{-1}), ν is the kinematic viscosity of the solution (0.01 cm^2 s^{-1}).[22,23] D_{O_2} is the diffusion coefficient of oxygen (1.9×10^{-5} cm^2 s^{-1}).[24,25] C_{O_2} is the concentration of oxygen in the bulk (1.13×10^{-6} mol cm^{-3}).[22,24]

3. RESULTS AND DISCUSSION

Structure and Morphology of GNR and N-GNR Composites. Figure 1 shows the preparation procedure of N-GNR nanomaterials, which were prepared by high-temperature pyrolysis of the GNR/PANI composite. GNR sheets with

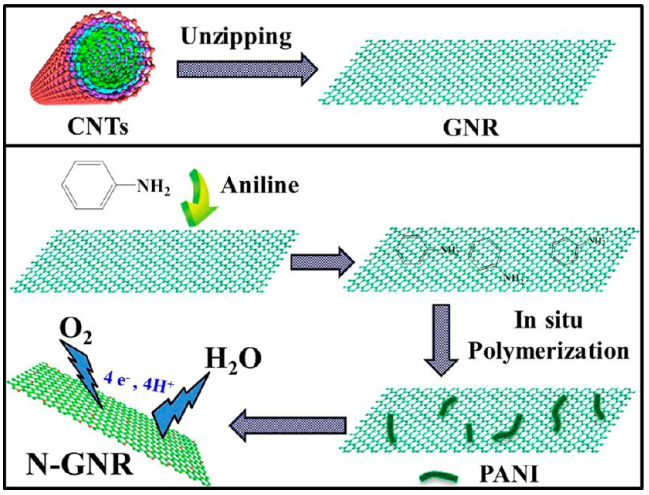

Figure 1. Schematic illustration of the synthetic procedure for N-GNR nanomaterials.

a high aspect ratio used in this work were prepared by longitudinally unzipping of the pristine CNTs. After being reduced by $N_2H_4{\cdot}H_2O$, a certain amount of the oxygen-containing groups can be removed. Then the GNR sheets were dispersed in DI water with the aid of ultrasonication. Different amounts of aniline solution (3 mM) in 0.1 M HCl were added into the GNR dispersion with APS as the catalyst. During the procedure of in situ polymerization, a GNR sheet acts as the structural framework so that a uniform layer of PANI was coated on its surface, which results in the formation of the GNR/PANI composite. N-GNR nanomaterials can be obtained after GNR/PANI composites were pyrolyzed at 900 °C for 1 h.

Figure 2 shows the TEM images of pristine CNTs, pure GNR sheets, neat PANI nanorods, and GNR/PANI composites. Pristine CNTs with a diameter of 30−50 nm were shown in Figure 2a. After the CNTs have been unzipped, GNR sheets with a larger width and a comparable length compared with the pristine CNTs have been obtained, as seen in Figure 2b. It can be seen that there are no residual CNTs existing in the obtained GNR material, indicating that the pristine CNTs were totally unzipped or opened. The successful unzipping of pristine CNTs has been further confirmed by XRD characterization. As seen in Figure S1, pristine CNTs show a sharp diffraction peak at $2\theta = 26.1°$, corresponding to a *d*-spacing of 3.4 Å which is a characteristic interlayer spacing of CNTs. After being unzipped, the obtained oxide GNR sheets show a broad diffraction peak centered at $2\theta = 12.1°$ (in the absence of residual diffraction at $2\theta = 26.1°$), corresponding to a *d*-spacing of 7.6 Å, confirming that the layer distance has been totally enlarged to 7.6 Å. These results can adequately indicate the pristine CNTs have been unzipped. In addition, the GNR sheets were bonded by each other with an enlarged contacting area. These unique structural characteristics can facilitate the formation of an electrical conductive pathway inside the prepared GNR sheets. Figure 2c shows the neat PANI prepared at the same process without the addition of GNRs. It can be seen that the obtained PANI nanorods show a hierarchical structure and similar size and/or length with the prepared GNR sheets. These features make it difficult to distinguish GNRs from PANI in the composite of GNR/PANI, as seen in Figure 2d. However, viewed from the overall aspect of the image, it can be seen that the GNR sheets and PANI nanorods are uniformly codispersed without apparent stacking or aggregation. Figure S2 shows the TEM and SEM images of GNR sheets and GNR/PANI composites, respectively, with large scale bars. This indicates that PANI nanorods can be uniformly deposited on the surface of GNRs, which makes sure a homogeneous doping of nitrogen element on the surface of GNR sheets and accelerates the catalytic ability of N-GNR nanomaterials.

The morphology of the prepared samples was further observed by SEM, as seen in Figure 3. Compared with the

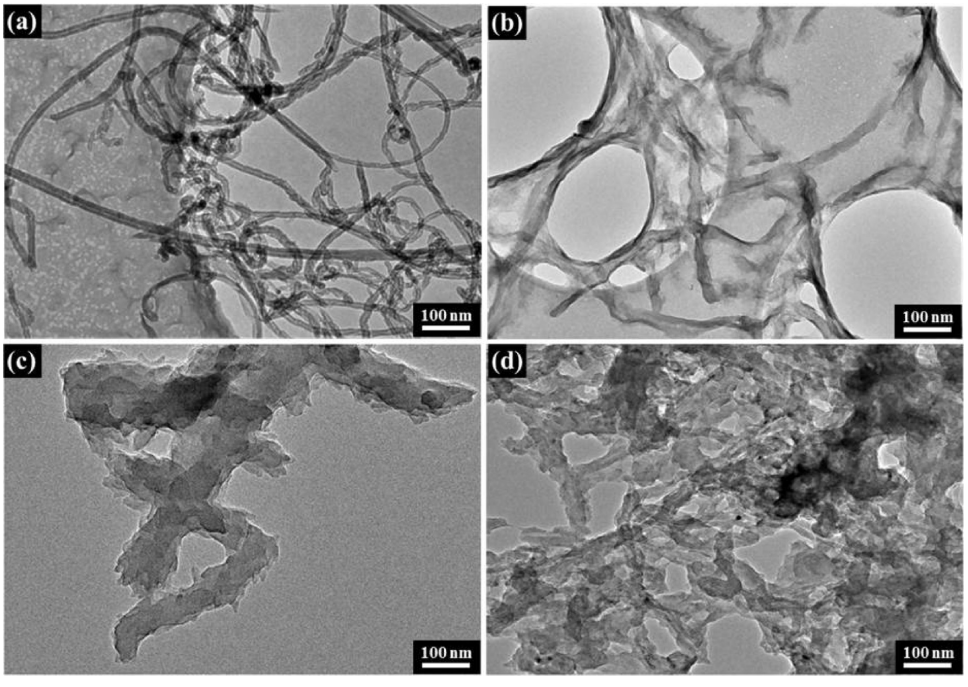

Figure 2. TEM images of (a) pristine CNTs, (b) pure GNR sheets, (c) neat PANI nanorods, and (d) GNR/PANI composites.

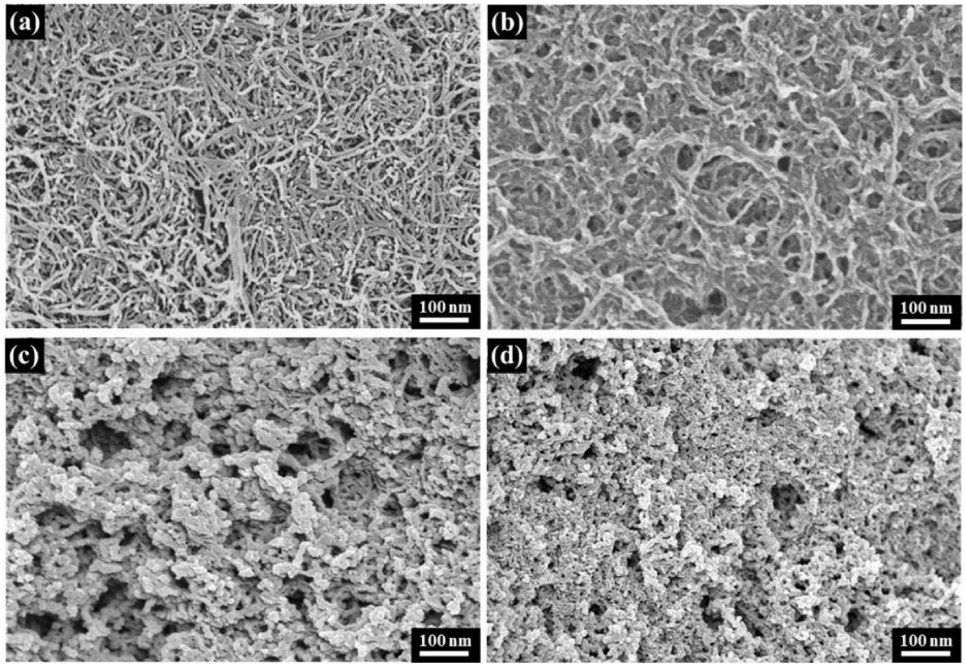

Figure 3. SEM images of (a) pristine CNTs, (b) pure GNR sheets, (c) neat PANI nanorods, and (d) GNR/PANI composites.

pristine CNTs (Figure 3a), the GNR sheets clearly exhibit a larger width, and uniform pores with a diameter of 30−50 nm were formed throughout the GNR nanomaterials. Furthermore, no tubelike CNTs can be observed all over the surface or structure of GNR sheets, which evidently confirms that the pristine CNTs have been successfully unzipped. Figure 3c shows the SEM image of neat PANI with a rodlike particle morphology, which seems to be loosely packed with pores existing inside it. Here, the unconspicuous difference of GNRs and PANI can be ascribed to the reasons that rodlike PANI has similar size and/or dimension compared with GNR sheets as well as low dimensional features of the GNRs. It can be also proposed that the GNR sheets prepared from unzipping the pristine CNTs have a certain amount of oxygen-containing groups on its surface that the aniline monomers are prone to be adsorbed on its surface due to the electrostatic interaction, which results in the layer-by-layer stacking of PANI nanorods on the surface of GNR sheets. This feature can facilitate the attachment and doping effect of the nitrogen element at the defective structure of GNR sheets.

Spectroscopic methods have been utilized to further confirm the structural evolution as the PANI content increases in GNR/PANI composites. Figure S3 shows the FTIR spectra of GNR sheets, pure PANI, and GNR/PANI composites with different weight percentages of PANI. As can be seen, the FTIR spectra of GNRs show weak absorption peaks centered at 1040 and 1720 cm^{-1}, corresponding to low content of C−OH and C═O groups. The relatively strong absorption peak at 3440 cm^{-1} can be ascribed to the vibration of −OH. Compared with the characteristic peak of PANI at about 857 and 1172 cm^{-1}, it can be found that the functional groups of PANI on the surface of GNRs are gradually increased, indicating that PANI was grown on the surface of GNRs in a layer-by-layer way, and for the sample of $GNR/PANI_{200}$, it is different to observe the characteristic peaks of GNRs as it shows almost the same absorption peaks of PANI, indicating the presence of PANI nanorods covered the surface of GNRs, which is consistent with the results of SEM observation.

Figure 4 shows the XRD patterns of pure GNRs, neat PANI, and GNR/PANI composites with different contents of PANI.

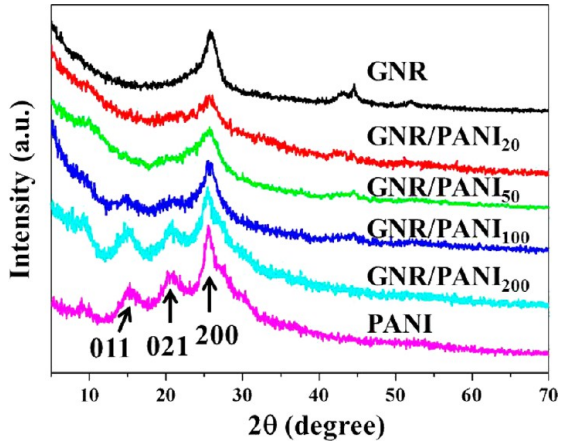

Figure 4. XRD curves of pure GNRs, neat PANI, and GNR/PANI composites with different contents of PANI.

The pattern of GNR exhibits a broad peak at 2θ = 25.6°, corresponding to a *d*-spacing of 3.46 Å. This result means that the interlayer spacing of GNR sheets was decreased as a certain amount of oxygen-containing groups have been removed, which is consistent with the XRD results of graphene sheets.[26] GNR/PANI composites show the gradually increased characteristic diffraction peaks of PANI as the PANI nanorods were deposited on the surface or interlayer of GNRs in a step-by-step way. In particular, the $GNR\text{-}PANI_{200}$ sample shows apparent characteristic diffraction peaks at 2θ = 14.9°, 20.6°, and 25.4°, corresponding to (011), (021), and (200) planes of the emeraldine salt form of PANI, respectively. These results further prove that PANI nanorods are deposited on the surface

dx.doi.org/10.1021/am405900r | ACS Appl. Mater. Interfaces 2014, 6, 4214−4222

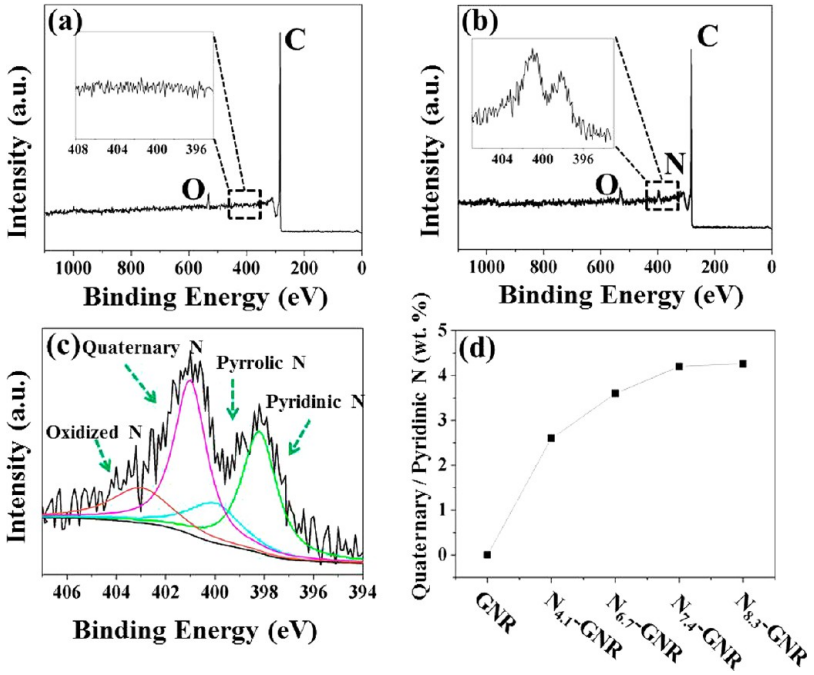

Figure 5. XPS analysis of (a) pure GNR sheets and (b) $N_{7.6}$-GNR. Inset: high resolution N 1s spectrum. (c) Peak deconvolutions of the N 1s spectra of $N_{8.3}$-GNR. (d) Quaternary N and pyridinic N content in the GNR sheets and N-GNR samples.

or interlayers of GNR sheets, which ensures the effective and efficient doping of nitrogen element at the plane of GNRs.

The obtained GNR/PANI composites have been treated with high-temperature pyrolysis in order to achieve the nitrogen doping effect of GNR sheets.[27] XPS experiments have been used to determine the surface element constitution of GNR sheets. As seen in Figure 5a, the survey spectrum of pure GNR sheets shows the presence of O and C peaks without any other impurities, indicating that a few oxygen-containing groups exist on GNR sheets which will assist the dispersion of GNRs. However, it is evident that no nitrogen element exists on the plane of GNR sheets as seen in the enlarged range from 395 to 408 eV (inset picture in Figure 5a). From the inset of Figure 5b, electron spectroscopy of nitrogen element was clearly observed in the range from 395 to 408 eV, indicating an efficient nitrogen doping effect of the GNR sheets.

The material property and performance to ORR strongly depend on the bonding configuration of N atoms in graphene or other carbon materials.[28] Generally, the nitrogen bonding configuration of nitrogen functionalities includes N atoms doped into a graphene basal plane (quaternary N), N atoms in a six-member ring (pyridinic N) and a five-member ring (pyrrolic N), and N atoms bonded with O atoms (oxidized N), as schematically shown in Figure 6. Here, the nitrogen contents in the GNR sheets are found to be 4.1, 6.7, 7.4, and 8.3 wt % (labeled as $N_{4.1}$-GNR, $N_{6.7}$-GNR, $N_{7.4}$-GNR, and $N_{8.3}$-GNR, respectively) for GNR-$PANI_{20}$, GNR-$PANI_{50}$, GNR-$PANI_{100}$, and GNR-$PANI_{200}$, which were prepared by polymerizing 20, 50, 100, and 200 mg of aniline monomer on the surface of 100 mg GNRs. The high-resolution N1s XPS spectrum of $N_{8.3}$-GNR was used primarily to determine the bonding configurations of N atoms in the composite, as seen in Figure 5c. The peak deconvolution suggests four components were centered at about 398.2, 400.0, 401.0, and 403.0 eV, corresponding to pyridinic N, pyrrolic N, quaternary N, and oxidized N, respectively.[20,29] As quaternary N and pyridinic N

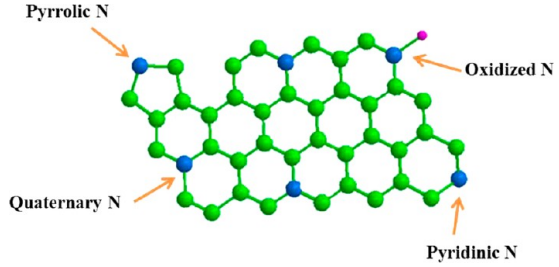

Figure 6. Schematic showing bonding configurations of N functionalities in N-GNR nanomaterial.

are crucial for the high catalytic activity of the carbon materials by playing the role of "active sites",[12,30] the contents of quaternary N and pyridinic N in the N-GNR samples have been calculated, as seen in Figure 5d. Quaternary N and pyridinic N contents in N-GNR samples were gradually increased with the increase of the PANI content in the GNR/PANI composites. This can be ascribed that positively charged PANI is prone to be bonded on the surface of negatively charged GNRs, and the nitrogen element tends to be doped at the defective structure, resulting in the formation of N-GNRs. Also, with the increase of PNAI content, more active sites in the GNR sheets can be created. However, due to its loosely stacking condition, some PANI located at the outside position can hardly contribute to the N doping efficiency, which can be also explained by the slight increase of quaternary and pyridinic N of $N_{8.3}$-GNR compared to that of $N_{7.4}$-GNR.

Raman spectroscopy is regarded as one of the most widely used techniques to characterize the structural derivation and electronic property of carbon materials including an element doping level.[31] In this work, the structural changes of GNRs, N-GNR nanomaterials obtained by cleavage of GNR/PANI composites were further investigated by Raman spectroscopy, as seen in Figure 7. Generally, the Raman spectrum of graphene or graphene-based materials is characterized by two main

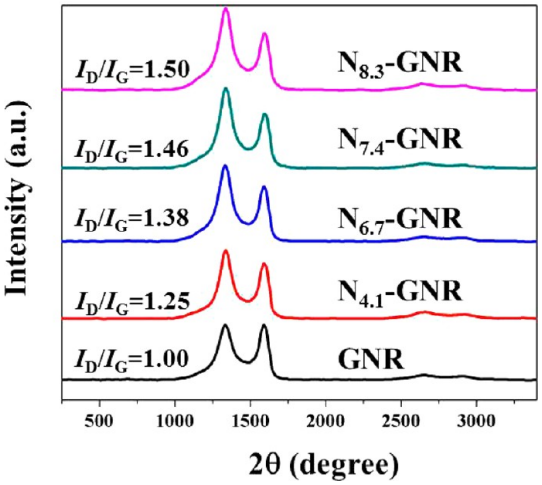

Figure 7. Raman spectra of pure GNR sheets, N-GNR nanomaterials with different N contents.

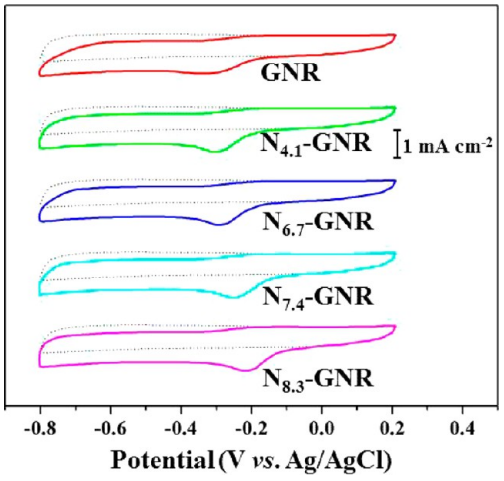

Figure 8. Cyclic voltammograms of GNRs, $N_{4.1}$-GNR, $N_{6.7}$-GNR, $N_{7.4}$-GNR, and $N_{8.3}$-GNR in the O_2-saturated (dashed curves) and the N_2-saturated (solid curves) KOH solution (0.1 mol/L).

features, including the D band arising from a breathing mode of *K*-point photons of A_{1g} symmetry and the G band arising from the first-order scattering of the E_{2g} phonon of sp^2 C atoms.[31] Compared with GNRs, the obtained N-GNR nanomaterials exhibit an enhanced intensity ratio of the D band and the G band (I_D/I_G, 1.50 for $N_{8.3}$-GNR compared with 1.00 for GNRs). These results can be ascribed to the size decrease of the sp^2 framework domain induced by high-temperature reduction and the doping effect induced by the pyrolysis of increased PANI content. This phenomenon can evidently prove that the doping role of PANI has been achieved during its structural decomposition as N-containing groups in PANI are prone to be cleaved and doped on carbonic materials at temperatures higher than 350 °C.[20] In addition, Raman spectrum of the annealed neat PANI powder with a I_D/I_G value of 1.0 has been obtained, as seen in Figure S4. The D band with a low intensity at 1324 cm^{-1} indicates that the PANI tends to be carbonized at high temperature with nitrogen containing groups recombined, resulting in the formation of a more stable structure and the loss of active sites for ORR.

Electrochemical Properties of GNR and N-GNR Composites. In order to adequately understand the ORR performance of GNRs and N-GNR nanomaterials, cyclic voltammograms (CV) of GNRs, $N_{4.1}$-GNR, $N_{6.7}$-GNR, $N_{7.4}$-GNR, and $N_{8.3}$-GNR in O_2-saturated and N_2-saturated KOH electrolytes were performed in a conventional three-electrode system, as shown in Figure 8. The GNR catalyst shows a pure capacitive current background in the N_2-saturated electrolyte and a relative broad cathodic peak at −0.31 V in the O_2-saturated electrolyte, indicating a good O_2 reduction property.[32] In contrast, the $N_{8.3}$-GNR nanomaterial catalyst shows a much more positive cathodic peak at −0.21 V and a higher cathodic current, suggesting an enhanced ORR catalytic activity of N-doped GNR sheets.[33−35]

To further evaluate the electrocatalytic activity of N-GNR nanomaterials, linear-sweep voltammetry (LSV) of GNRs and N-GNR nanomaterials at a rotation speed of 1600 rpm was also measured in the O_2-saturated 0.1 mol/L KOH solution on RDE, as seen in Figure 9a. Clearly, the N-GNR nanomaterials exhibit much higher current density compared with the GNR catalyst, indicating a greatly enhanced activity for ORR by the introduction of the N element. Especially, the nanomaterial of $N_{8.3}$-GNR shows a much more positive onset potential than the other prepared samples including the GNR catalyst, which reveals that the catalytic activity of $N_{8.3}$-GNR is promising and outstanding. Furthermore, a set of LSV curves for ORR based on the $N_{8.3}$-GNR catalyst recorded from 400 to 2400 rpm was shown in Figure 9b. It can be seen that the measured current density was gradually increased with the increase of rotation rate, which can be explained that the diffusion distance at high speeds was shortened. The Koutecky−Levich plots (J^{-1} vs $\omega^{-1/2}$) were obtained from the polarization curves at different potentials, as seen in Figure 9c. The good linearity of the Koutecky−Levich plots and nearly parallelism of the fitting lines suggest first-order reaction kinetics toward the concentration of dissolved oxygen and similar electron transfer number for ORR at different potentials.[36,37] Here, the transferred electron number (n) per O_2 from the slopes of Koutecky−Levich plots as $N_{8.3}$-GNR is calculated to be 3.91 at potentials from −0.15 to −0.3 V. This suggests that the catalyst of $N_{8.3}$-GNR exhibits a dominant four-electron oxygen reduction process, as seen in Figure S5. In contrast, GNR sheets without N doping exhibit an electron transfer number of 2.89, indicating a combined two-electron and four-electron reduction pathway.[38] In addition, the kinetic-limiting current density (J_K) calculated from the linearity of J^{-1} vs $\omega^{-1/2}$ is 5.15 for $N_{8.3}$-GNR, which is comparable or even higher than previously reported results for nitrogen-doped graphene, CNTs, and other types of carbon materials,[24] as seen in Figure 9d. This excellent performance of electrocatalytic activity can be indicated that, as the obtained GNR sheets have straight ribbonlike structure, most N atoms doped on its surface are quaternary N and pyridinic N, and oxygen molecules can be activated on both of these two kinds of doped N. As for quaternary N, electrons transfer from the adjacent C to N atoms, and N donates back electrons to adjacent C p_z orbitals, and the donation and back-donation process will not only facilitate O_2 dissociation on the adjacent C atoms but also help to form a strong chemical bond between O and C.[28] Also for pyridinic N located at the GNR edge, oxygen can be activated via direct bonding with the lone electron pair of N.[39] Furthermore, the durability of $N_{8.3}$-GNR and Pt/C catalysts toward ORR was evaluated through chronoamperometric measurements at −0.3 V, as shown in Figure 10. After 5000 s, the $N_{8.3}$-GNR lost 4.9% of its initial catalytic activity

dx.doi.org/10.1021/am405900r | ACS Appl. Mater. Interfaces 2014, 6, 4214−4222

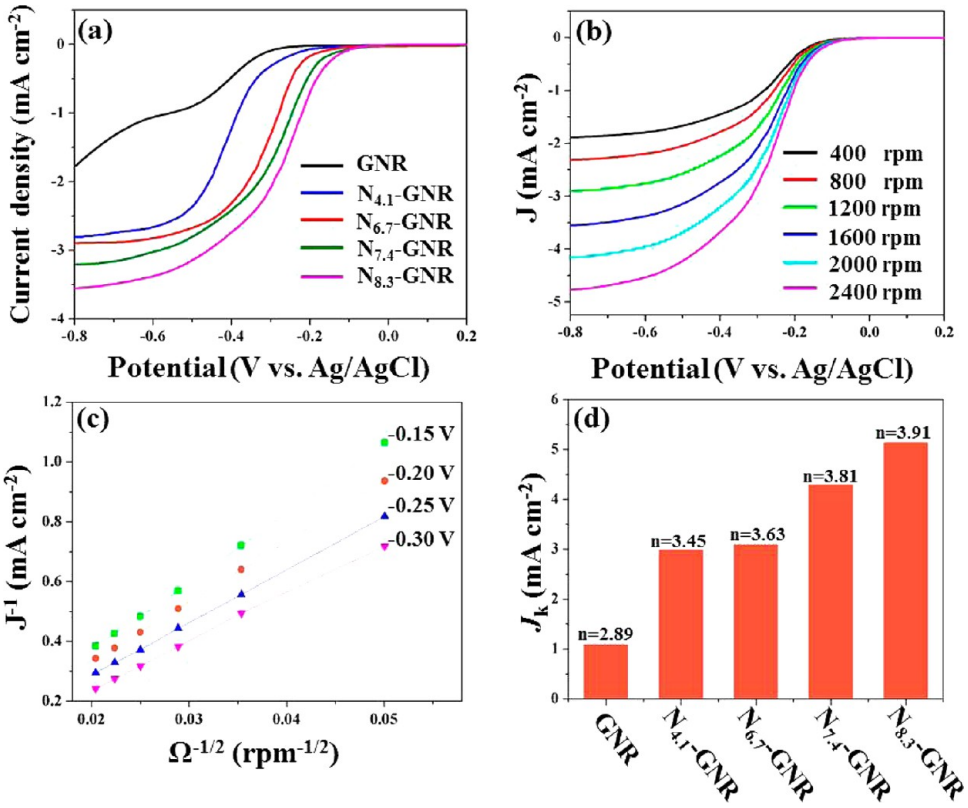

Figure 9. (a) RDE curves of ORR for GNR and N-GNR nanomaterials in the O_2-saturated 0.1 mol/L KOH solution at a scan rate of 10 mV s^{-1} with an electrode rotation rate of 1600 rpm. (b) RED curves for $N_{8.3}$-GNR in the O_2-saturated 0.1 mol/L KOH solution at a scan rate of 10 mV s^{-1} with different rotation rates from 400 to 2400 rpm. (c) Koutecky–Levich plots of J^{-1} vs $\omega^{-1/2}$ at different potentials derived from the RDE measurements. (d) Electrochemical activity given as the kinetic-limiting current density (J_K) at −0.7 V for GNR and N-GNR nanomaterials.

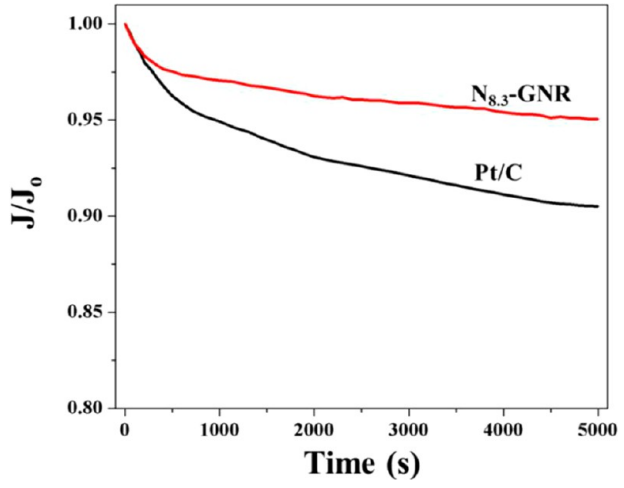

Figure 10. Chronoamperometric responses of the $N_{8.3}$-GNR nanomaterial and the Pt/C catalyst at −0.3 V in the O_2-saturated 0.1 M KOH electrolyte.

compared with 9.5% of Pt/C. This means a much better stability of $N_{8.3}$-GNR than the commercial Pt/C catalyst in alkaline solution, which is an exciting result for the further applications in alkaline fuel cells. All these results clearly demonstrate that the N-GNR nanomaterials prepared in this work are promising metal-free catalysts for ORR with excellent electrocatalytic activity and very good stability, which can be a feasible alternative to Pt.

4. CONCLUSIONS

In this work, N-GNR with different N contents have been facilely prepared via high temperature pyrolysis of GNR/PANI composites, where the GNR sheets were prepared by longitudinally unzipping from the multiwalled CNTs. Due to the unique structure of GNRs, the N atoms decomposed or reconstructed from PANI are primarily quaternary N and pyridinic N, which are crucial for high performance of ORR. Compared with neat GNR sheets, the prepared $N_{8.3}$-GNR nanomaterial exhibits a much more positive onset potential in the polarization curve and the cathodic peak in the cyclic voltammogram with an almost four-electron transfer process of O_2 reduction, indicating a greatly enhanced catalyst activity for ORR. Also, $N_{8.3}$-GNR nanomaterial possesses a comparable stability with the commercial Pt/C. In addition to the promising performance at oxygen reduction, it can be anticipated that this N-GNR nanomaterial can provide wide applications in the field of supercapacitors, sensors, lithium ion batteries, and other energy storage and conversion.

■ ASSOCIATED CONTENT

Supporting Information

XRD patterns of pristine CNTs and oxide GNR sheets, TEM and SEM images of prepared samples with large scale bars, FTIR characterization of pure GNRs, neat PANI and GNR/PANI composites, Raman spectrum of annealed PANI powder, and schematic diagram showing the reduction of O_2 to H_2O by N-GNR. This material is available free of charge via the Internet at http://pubs.acs.org.

AUTHOR INFORMATION

Corresponding Author

*Phone: 86-21-55664197. Fax: 86-21-65640293. E-mail: txliu@fudan.edu.cn.

Notes

The authors declare no competing financial interest.

ACKNOWLEDGMENTS

The authors are grateful for the financial support from the National Natural Science Foundation of China (51125011).

REFERENCES

(1) Kosynkin, D. V.; Higginbotham, A. L.; Sinitskii, A.; Lomeda, J. R.; Dimiev, A.; Price, B. K.; Tour, J. M. Longitudinal Unzipping of Carbon Nanotubes To Form Graphene Nanoribbons. *Nature* **2009**, *458*, 872−875.

(2) Yang, X. Y.; Dou, X.; Rouhanipour, A.; Zhi, L. J.; Rader, H. J.; Mullen, K. Two-Dimensional Graphene Nanoribbons. *J. Am. Chem. Soc.* **2008**, *130*, 4216−4217.

(3) Tapaszto, L.; Dobrik, G.; Lambin, P.; Biro, L. P. Tailoring the Atomic Structure of Graphene Nanoribbons by Scanning Tunneling Microscope. *Nat. Nanotechnol.* **2008**, *3*, 397−401.

(4) Ci, L.; Xu, Z. P.; Wang, L. L.; Gao, W.; Ding, F.; Kelly, K. F.; Yakobson, B. I.; Ajayan, P. M. Controlled Nanocutting of Graphene. *Nano Res.* **2008**, *1*, 116−122.

(5) Campos-Delgado, J.; Romo-Herrera, J. M.; Jia, X. T.; Cullen, D. A.; Muramatsu, H.; Kim, Y. A.; Hayashi, T.; Ren, Z. F.; Smith, D. J.; Okuno, Y.; Ohba, T.; Kanoh, H.; Kaneko, K.; Endo, M.; Terrones, H.; Dresselhaus, M. S.; Terrones, M. Bulk Production of a New Form of sp^2 Carbon: Crystalline Graphene Nanoribbons. *Nano Lett.* **2008**, *8*, 2773−2778.

(6) Rafiee, M. A.; Lu, W.; Thomas, A. V.; Zandiatashbar, A.; Rafiee, J.; Tour, J. M.; Koratkar, N. A. Graphene Nanoribbon Composites. *ACS Nano* **2010**, *4*, 7415−7420.

(7) Higginbotham, A. L.; Kosynkin, D. V.; Sinitskii, A.; Sun, Z. Z.; Tour, J. M. Lower-Defect Graphene Oxide Nanoribbons from Multiwalled Carbon Nanotubes. *ACS Nano* **2010**, *4*, 2059−2069.

(8) Yan, Q. M.; Huang, B.; Yu, J.; Zheng, F. W.; Zang, J.; Wu, J.; Gu, B. L.; Liu, F.; Duan, W. H. Intrinsic Current-Voltage Characteristics of Graphene Nanoribbon Transistors and Effect of Edge Doping. *Nano Lett.* **2007**, *7*, 1469−1473.

(9) Son, J. G.; Son, M.; Moon, K. J.; Lee, B. H.; Myoung, J. M.; Strano, M. S.; Ham, M. H.; Ross, C. A. Sub-10 nm Graphene Nanoribbon Array Field-effect Transistors Fabricated by Block Copolymer. *Adv. Mater.* **2013**, *25*, 4723−4728.

(10) He, H. Y.; Li, X. L.; Wang, J.; Qiu, T. F.; Fang, Y.; Song, Q.; Luo, B.; Zhang, X. F.; Zhi, L. J. Reduced Graphene Oxide Nanoribbon Networks: A Novel Approach towards Scalable Fabrication of Transparent Conductive Films. *Small* **2013**, *9*, 820−824.

(11) Wu, M. H.; Gao, Y.; Zhang, Z. Y.; Zeng, X. C. Edge-Decorated Graphene Nanoribbons by Scandium as Hydrogen Storage Media. *Nanoscale* **2012**, *4*, 915−920.

(12) Zheng, Y.; Jiao, Y.; Jaroniec, M.; Jin, Y. G.; Qiao, S. Z. Nanostructured Metal-Free Electrochemical Catalysts for Highly Efficient Oxygen Reduction. *Small* **2012**, *8*, 3550−3566.

(13) Yang, L. J.; Jiang, S. J.; Zhao, Y.; Zhu, L.; Chen, S.; Wang, X. Z.; Wu, Q.; Ma, J.; Ma, Y. W.; Hu, Z. Boron-Doped Carbon Nanotubes as Metal-Free Electrocatalysts for the Oxygen Reduction Reaction. *Angew. Chem., Int. Ed.* **2011**, *50*, 7132−7135.

(14) Wang, Y.; Shao, Y. Y.; Matson, D. W.; Li, J. H.; Lin, Y. H. Nitrogen-Doped Graphene and Its Application in Electrochemical Biosensing. *ACS Nano* **2010**, *4*, 1790−1798.

(15) Huang, L.; Yi, N.; Wu, Y.; Zhang, Y.; Zhang, Q.; Huang, Y.; Ma, Y. F.; Chen, Y. S. Multichannel and Repeatable Self-Healing of Mechanical Enhanced Graphene-Thermoplastic Polyurethane Composites. *Adv. Mater.* **2013**, *25*, 2224−2228.

(16) Liang, J. J.; Huang, Y.; Oh, J. Y.; Kozlov, M.; Sui, D.; Fang, S. L.; Baughman, R. H.; Ma, Y. F.; Chen, Y. S. Electromechanical Actuators Based on Graphene and Graphene/Fe_3O_4 Hybrid Paper. *Adv. Funct. Mater.* **2011**, *21*, 3778−3784.

(17) Panchalkarla, L. S.; Govindaraj, A.; Rao, C. Nitrogen- and Boron-Doped Double-Walled Carbon Nanotubes. *ACS Nano* **2007**, *1*, 494−500.

(18) Deng, D. H.; Pan, X. L.; Yu, L. A.; Cui, Y.; Jiang, Y. P.; Qi, J.; Li, W. X.; Fu, Q. A.; Ma, X. C.; Xue, Q. K.; Sun, G. Q.; Bao, X. H. Toward N-Doped Graphene via Solvothermal Synthesis. *Chem. Mater.* **2011**, *23*, 1188−1193.

(19) Gong, K. P.; Du, F.; Xia, Z. H.; Durstock, M.; Dai, L. M. Nitrogen-Doped Carbon Nanotube Arrays with High Electrocatalytic Activity for Oxygen Reduction. *Science* **2009**, *323*, 760−764.

(20) Lin, Z. Y.; Waller, G. H.; Liu, Y.; Liu, M. L.; Wong, C. P. Simple Preparation of Nanoporous Few-Layer Nitrogen-Doped Graphene for Use As an Efficient Electrocatalyst for Oxygen Reduction and Oxygen Evolution Reactions. *Carbon* **2013**, *53*, 130−136.

(21) Li, Y. G.; Zhou, W.; Wang, H. L.; Xie, L. M.; Liang, Y. Y.; Wei, F.; Idrobo, J. C.; Pennycook, S. J.; Dai, H. J. An Oxygen Reduction Electrocatalyst Based on Carbon Nanotube-Graphene Complexes. *Nat. Nanotechnol.* **2012**, *7*, 394−400.

(22) Zhong, R. S.; Qin, Y. H.; Niu, D. F.; Tian, J. W.; Zhang, X. S.; Zhou, X. G.; Sun, S. G.; Yuan, W. K. Effect of Carbon Nanofiber Surface Functional Groups on Oxygen Reduction in Alkaline Solution. *J. Power Sources* **2013**, *225*, 192−199.

(23) Chen, W.; Chen, S. W. Oxygen Electroreduction Catalyzed by Gold Nanoclusters: Strong Core Size Effects. *Angew. Chem., Int. Ed.* **2009**, *48*, 4386−4389.

(24) Roche, I.; Chainet, E.; Chatenet, M.; Vondrak, J. Carbon-Supported Manganese Oxide Nanoparticles as Electrocatalysts for the Oxygen Reduction Reaction (ORR) in Alkaline Medium: Physical Characterizations and ORR Mechanism. *J. Phys. Chem. C* **2007**, *111*, 1434−1443.

(25) Ahmed, M. S.; Jeon, S. New Functionalized Graphene Sheets for Enhanced Oxygen Reduction as Metal-Free Cathode. *J. Power Sources* **2012**, *218*, 168−173.

(26) Parvez, K.; Yang, S. B.; Hernandez, Y.; Winter, A.; Turchanin, A.; Feng, X. L.; Mullen, K. Nitrogen-Doped Graphene and Its Iron-Based Composite As Efficient Electrocatalysts for Oxygen Reduction Reaction. *ACS Nano* **2012**, *6*, 9541−9550.

(27) Wu, G.; More, K. L.; Johnston, C. M.; Zelenay, P. High-Performance Electrocatalysts for Oxygen Reduction Derived from Polyaniline, Iron, and Cobalt. *Science* **2011**, *332*, 443−447.

(28) Wang, X. R.; Li, X. L.; Zhang, L.; Yoon, Y. K.; Weber, P. K.; Wang, H. L.; Guo, J.; Dai, H. J. N-Doping of Graphene through Electrothermal Reactions with Ammonia. *Science* **2009**, *324*, 768−771.

(29) Qu, L. T.; Liu, Y.; Baek, J. B.; Dai, L. M. Nitrogen-Doped Graphene as Efficient Metal-Free Electrocatalyst for Oxygen Reduction in Fuel Cells. *ACS Nano* **2010**, *4*, 1321−1326.

(30) Zhang, L. P.; Xia, Z. H. Mechanisms of Oxygen Reduction Reaction on Nitrogen-Doped Graphene for Fuel Cells. *J. Phys. Chem. C* **2011**, *115*, 11170−11176.

(31) Kundu, S.; Nagaiah, T. C.; Xia, W.; Wang, Y. M.; Van Dommele, S.; Bitter, J. H.; Santa, M.; Grundmeier, G.; Bron, M.; Schuhmann, W.; Muhler, M. Electrocatalytic Activity and Stability of Nitrogen-containing Carbon Nanotubes in the Oxygen Reduction Reaction. *J. Phys. Chem. C* **2009**, *113*, 14302−14310.

(32) Chen, S.; Bi, J. Y.; Zhao, Y.; Yang, L. J.; Zhang, C.; Ma, Y. W.; Wu, Q.; Wang, X. Z.; Hu, Z. Nitrogen-Doped Carbon Nanocages as Efficient Metal-Free Electrocatalysts for Oxygen Reduction Reaction. *Adv. Mater.* **2012**, *24*, 5593−5597.

(33) Nagaiah, T. C.; Kundu, S.; Bron, M.; Muhler, M.; Schuhmann, W. Nitrogen-Doped Carbon Nanotubes as a Cathode Catalyst for the Oxygen Reduction Reaction in Alkaline Medium. *Electrochem. Commun.* **2010**, *12*, 338−341.

(34) Kim, H.; Lee, K.; Woo, S. I.; Jung, Y. On the Mechanism of Enhanced Oxygen Reduction Reaction in Nitrogen-doped Graphene Nanoribbons. *Phys. Chem. Chem. Phys.* **2011**, *13*, 17505−17510.

(35) Studt, F. The Oxygen Reduction Reaction on Nitrogen-Doped Graphene. *Catal. Lett.* **2013**, *143*, 58−60.
(36) Tan, Y. M.; Xu, C. F.; Chen, G. X.; Fang, X. L.; Zheng, N. F.; Xie, Q. J. Facile Synthesis of Manganese-oxide-containing Mesoporous Nitrogen-Doped Carbon for Efficient Oxygen Reduction. *Adv. Funct. Mater.* **2012**, *22*, 4584−4591.
(37) Liang, Y. Y.; Li, Y. G.; Wang, H. L.; Zhou, J. G.; Wang, J.; Regier, T.; Dai, H. J. Co_3O_4 Nanocrystals on Graphene as a Synergistic Catalyst for Oxygen Reduction Reaction. *Nat. Mater.* **2011**, *10*, 780−786.
(38) Chen, T.; Cai, Z. B.; Yang, Z. B.; Li, L.; Sun, X. M.; Huang, T.; Yu, A. S.; Kia, H. G.; Peng, H. S. Nitrogen-doped Carbon Nanotube Composite Fiber with a Core-Sheath Structure for Novel Electrodes. *Adv. Mater.* **2011**, *23*, 4620−4625.
(39) Geng, D. S.; Liu, H.; Chen, Y. G.; Li, R. Y.; Sun, X. L.; Ye, S. Y.; Knights, S. Non-Noble Metal Oxygen Reduction Electrocatalysts Based on Carbon Nanotubes with Controlled Nitrogen Contents. *J. Power Sources* **2011**, *196*, 1795−1801.